J. metamorphic Geol., 2004, **22,** 301–313 doi:10.1111/j.1525-1314.2004.00515.x

Metamorphic evolution of kyanite–staurolite-bearing epidote–amphibolite from the Early Palaeozoic Oeyama belt, SW Japan

T. TSUJIMORI[1,2] AND J. G. LIOU[2]

[1]*Research Institute of Natural Sciences, Okayama University of Science, Okayama 700–0005, Japan (tatsukix@pangea.stanford.edu)*

[2]*Department of Geological and Environmental Sciences, Stanford University, Stanford, CA 94305, USA*

ABSTRACT Early Palaeozoic kyanite–staurolite-bearing epidote–amphibolites including foliated epidote–amphibolite (FEA), and nonfoliated leucocratic or melanocratic metagabbros (LMG, MMG), occur in the Fuko Pass metacumulate unit (FPM) of the Oeyama belt, SW Japan. Microtextural relationships and mineral chemistry define three metamorphic stages: relict granulite facies metamorphism (M1), high-*P* (HP) epidote–amphibolite facies metamorphism (M2), and retrogression (M3). M1 is preserved as relict Al-rich diopside (up to 8.5 wt.% Al_2O_3) and pseudomorphs after spinel and plagioclase in the MMG, suggesting a medium-*P* granulite facies condition (0.8–1.3 GPa at > 850 °C). An unusually low-variance M2 assemblage, Hbl + Czo + Ky ± St + Pg + Rt ± Ab ± Crn, occurs in the matrix of all rock types. The presence of relict plagioclase inclusions in M2 kyanite associated with clinozoisite indicates a hydration reaction to form the kyanite-bearing M2 assemblage during cooling. The corundum-bearing phase equilibria constrain a qualitative metamorphic *P–T* condition of 1.1–1.9 GPa at 550–800 °C for M2. The M2 minerals were locally replaced by M3 margarite, paragonite, plagioclase and/or chlorite. The breakdown of M2 kyanite to produce the M3 assemblage at < 0.5 GPa and 450–500 °C suggests a greenschist facies overprint during decompression. The *P–T* evolution of the FPM may represent subduction of an oceanic plateau with a granulite facies lower crust and subsequent exhumation in a Pacific-type orogen.

Key words: Early Palaeozoic; epidote–amphibolite; kyanite; polyphase metamorphism; *P–T* path; staurolite.

INTRODUCTION

Amphibolites are common in many Barrovian-type metamorphic terranes. Most contain higher-variance mineral assemblages that do not constrain well the metamorphic conditions. However, some high-pressure (HP) amphibolites with an aluminous bulk-rock composition contain kyanite and staurolite (e.g. Gibson, 1979; Selverstone *et al.*, 1984; Yokoyama & Goto, 1987; Gil Ibarguchi *et al.*, 1991; Kuyumjian, 1998). Such unusual amphibolite assemblages are useful to constrain the *P–T* path (e.g. Arnold *et al.*, 2000) as reaction textures are well displayed in aluminous minerals such as kyanite (e.g. Spear & Franz, 1986; Cotkin *et al.*, 1988).

Early Palaeozoic kyanite- and staurolite-bearing epidote–amphibolite and metagabbro of the Fuko Pass metacumulate unit (FPM) occur in the peridotite body of Early Palaeozoic Oeyama belt (Kurokawa, 1975; Kuroda *et al.*, 1976; Tsujimori, 1999). The Ky–St-bearing rocks have been considered to have recrystallized at medium-*P* (*c.* 0.5 GPa), possibly in an ocean-floor setting, as a cumulate member of an ophiolitic succession (Kurokawa, 1985). On the other hand, the Hbl + Czo + Ky + Pg + Rt assemblage suggests HP metamorphism (Tsujimori, 1999). Moreover, medium-*P* granulite-facies relics of Al-rich diopside and pseudomorphs of spinel and plagioclase were recently identified in some metacumulate rocks (Tsujimori & Ishiwatari, 2002). These rocks constrain a unique metamorphic evolution from the granulite-facies to HP metamorphism. The occurrence of an Early Palaeozoic HP metamorphic event in the FPM may signify the earliest subduction-metamorphism in the Pacific-type orogen of the Japanese Islands.

This paper presents new petrological data for the Ky–St-bearing epidote–amphibolites and metagabbros of the FPM, which are coupled with previous data to evaluate a polyphase metamorphic evolution of the FPM and discuss the tectonic significance of this evolution. Mineral abbreviations are after Kretz (1983) and the term ‘hornblende (Hbl)’ is used to describe Ca-amphibole with dominantly pargasitic, tschermakitic and edenitic composition throughout this paper.

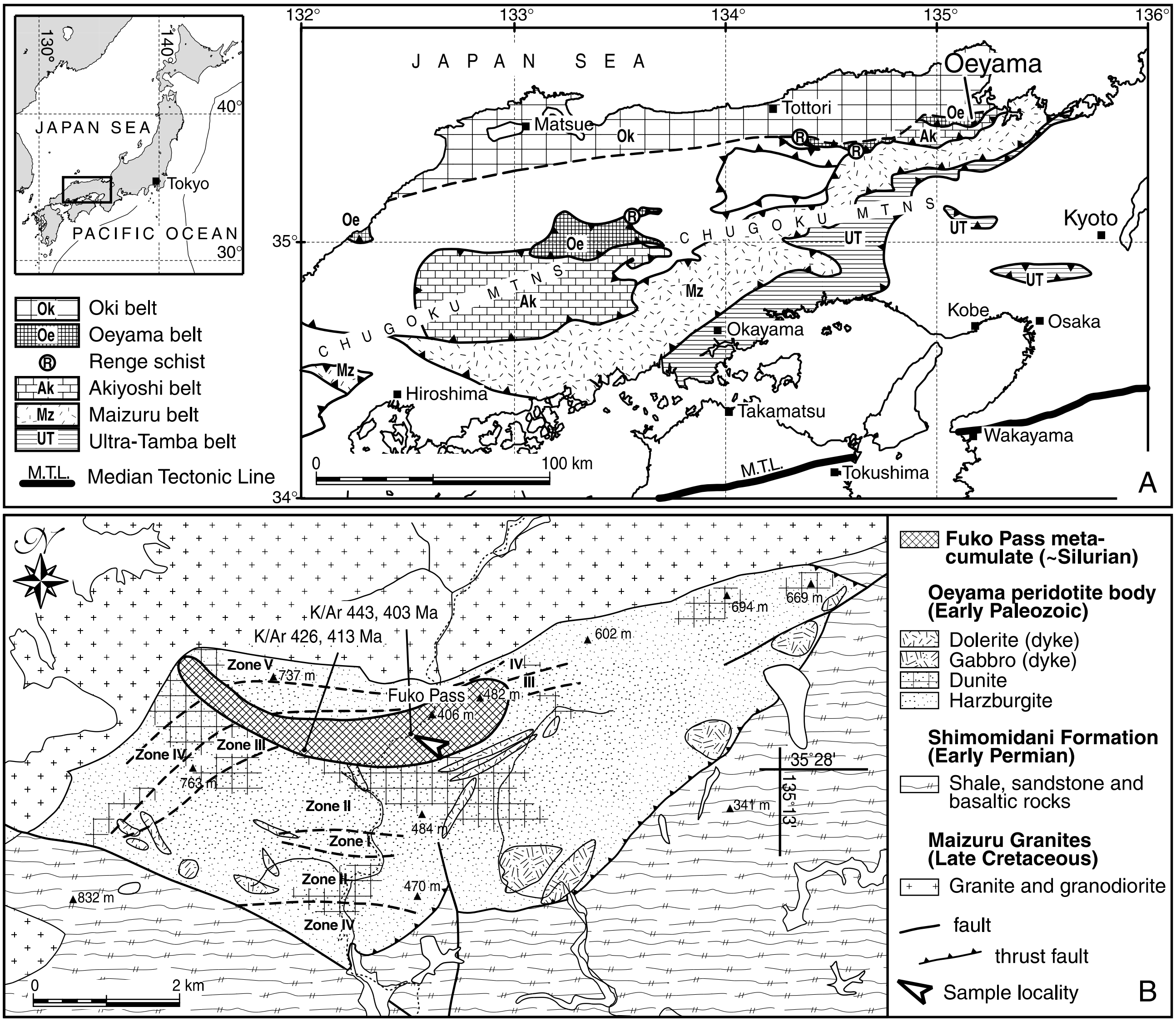

Fig. 1. (a) A simplified map of the Chugoku Mountains, showing various pre-Triassic petrotectonic units and the locality of the Oeyama area. (b) Geological map of the Oeyama area, showing sample locality of the Ky–St-bearing rocks (after Tsujimori *et al.*, 2000).

GEOLOGICAL SETTING

The Oeyama belt is an Early Palaeozoic ophiolitic nappe that occupies the highest structural position in the Phanerozoic Pacific-type orogen of south-west Japan (e.g. Ishiwatari & Tsujimori, 2003) (Fig. 1). Several serpentinized peridotite bodies in the Chugoku Mountains consist mainly of residual peridotite with minor gabbro dykes and podiform chromitites (Arai, 1980; Kurokawa, 1985; Matsumoto *et al.*, 1997). The peridotite has a lherzolitic composition in the eastern part, but is harzburgitic in the western part. The gabbro dykes have MORB-like affinity and yield Sm/Nd isochron ages of *c.* 560 Ma (Hayasaka *et al.*, 1995), suggesting a Cambrian or earlier age for the ophiolite formation. The Oeyama peridotite may have been derived from suprasubduction zone mantle beneath an intraoceanic arc (Tsujimori & Itaya, 1999; Ishiwatari & Tsujimori, 2003).

Two different HP mafic rocks are associated with serpentinized peridotite bodies in the Oeyama belt. The younger HP rocks consist of 330–280 Ma blueschist to eclogite facies metasediments and minor metabasalt, and represent fragments of the Late Palaeozoic Renge blueschist nappe underlying the Oeyama belt (Nishimura, 1998; Tsujimori, 1998; Tsujimori & Itaya, 1999). In contrast, the older HP rocks are characterized by 470–400 Ma deformed metagabbro and metaclinopyroxenite (Nishimura & Shibata, 1989; Tsujimori *et al.*, 2000). The FPM belongs to the latter type.

The FPM occurs as a fault-bounded slice at the topographically higher portion of the Oeyama peridotite body that tectonically overlies the Permian accretionary complex of the Akiyoshi belt (Fig. 1). The FPM is a meta-ultramafic–mafic complex consisting of metamorphosed clinopyroxenite, wehlrite and cumulate gabbro (Kurokawa, 1985). On the other hand, the Oeyama peridotite body is composed of fertile harzburgite with minor dolerite and gabbro dykes (Uda, 1984; Kurokawa, 1985). Both have been highly serpentinized, and subsequently significantly overprinted by contact metamorphism around Late Cretaceous granitic intrusions. Uda (1984) identified five contact metamorphic zones: I – Atg; II – Ol + Atg + Di; III – Ol + Atg + Tr; IV –Ol + Tlc ± Tr ± Cum; and V – Ol + En ± Tr ± Hbl. Primary igneous phases, Ol

(Fo_{90-91}) + Opx ($Al_2O_3 = 3.2–4.3$ wt.%) + Cpx ($Na_2O < 0.3$ wt.%) + Cr-Spl (Cr# = 0.34–0.38), are well preserved in Zone I rocks (Kurokawa, 1985; Tsujimori, 1999). The FPM extends from Zone II to Zone V; few outcrops lack the thermal effect of the contact metamorphism. No gabbro intrusions cut through the FPM, whereas the adjacent serpentinized peridotite was intruded by syn- or post-tectonic gabbroic rocks. Thus, it is interpreted that the FPM was tectonically juxtaposed with the Oeyama peridotite body. K/Ar hornblende ages of the FPM yield 443–403 Ma (Tsujimori *et al.*, 2000).

Samples were collected at an outcrop (20 × 3 m) near the Fuko Pass where the effect of contact metamorphism is minimal (Kurokawa, 1985). Ky–St-bearing rocks occur together with irregular blocks of massive coarse-grained metagabbro, virtually undeformed, in the matrix of foliated (or gneissose) epidote–amphibolite. Tsujimori (1999) used the term 'metagabbro' to indicate any undeformed epidote–amphibolite in which original gabbroic textures are well-preserved, and distinguished it from the 'foliated epidote–amphibolite'. The metagabbro is subdivided into leucocratic and melanocratic varieties by the content of clinozoisite.

ANALYTICAL METHODS

Concentrations of major (Si, Ti, Al, Fe, Mn, Mg, Ca, Na, K & P) and trace (Ni, Cu, Zn, Pb, Y & V) elements were analyzed by a Rigaku System 3270 X-ray fluorescence spectrometer with Rh tube at Kanazawa University. The operating conditions for both major and trace elements were 50 kV accelerating voltage and 20 mA beam current. Other trace elements (Sc, Cr, Co, La, Sm, Eu, Lu & Th) were determined by instrumental neutron activation analysis (INAA method). The INAA samples were activated at Kyoto University Reactor, and the gamma-ray spectroscopic analyses were done at the Radioisotope Laboratory of Kanazawa University.

Electron microprobe analysis was carried out with a JEOL JXA-8800R at Kanazawa University and JEOL JXA-8900R at Okayama University of Science. The quantitative analyses of rock-forming minerals were performed with 15 kV accelerating voltage, 12 nA beam current and 3–5 μm beam size. Natural and synthetic silicates and oxides were used for calibration. The ZAF method (oxide basis) was employed for matrix corrections.

PETROGRAPHY

Three rock types are distinguished according to their lithological and petrographical features: (1) foliated epidote–amphibolite (FEA); (2) leucocratic metagabbro (LMG); and (3) melanocratic metagabbro (MMG). Although epidote–amphibolite facies assemblages are dominant in all lithologies, each rock type preserves textual evidence for mineral growth during an earlier stage and of retrograde metamorphic events. Three metamorphic stages, M1, M2 and M3, are distinguished on the basis of microtextural relationships and mineral chemistry. Mineral parageneses for different metamorphic stages of these rock types are summarized in Fig. 2. *M*2 defines the peak HP metamorphism of all rock types, whereas *M*1 minerals are identified as relict minerals, particularly granulite facies relics and pseudomorphs in melanocratic metagabbro. *M*3 represents lower-*P* retrogression during decompression.

FEA: foliated epidote–amphibolite

This rock type consists mainly of hornblende, clinozoisite and kyanite with small amounts of paragonite, rutile, chlorite, margarite, staurolite, corundum, zoisite, and rare albite and muscovite. Ilmenite, sulphides and apatite occur as accessories. A foliation defined by preferred orientation of nematoblastic hornblende, kyanite and paragonite is developed. Mosaic aggregates of clinozoisite are intergrown with paragonite, kyanite, rutile, hornblende and staurolite; these minerals also occur as inclusions in clinozoisite (Fig. 3a,b). Rare zoisite blebs (< 0.1 mm), albite and muscovite are included in clinozoisite. Some staurolite (< 0.5 mm) occurs as aggregates (up to 5 mm) with minor corundum (< 0.1 mm) and rare magnetite; the aggregate is armoured by kyanite and clinozoisite at the margin (Fig. 3c). These matrix minerals and inclusions in clinozoisite are thought to be in textural equilibrium, and the mineral assemblage Hbl + Czo + Ky ± St + Pg + Rt ± Ab ± Crn characterizes the peak M2. Some kyanite crystals contain plagioclase as tiny inclusions (< 0.03 mm) (Fig. 3d); this may represent a precursor of the peak of M2, possibly a remnant of the M1 stage. Rutile contains exsolution blebs

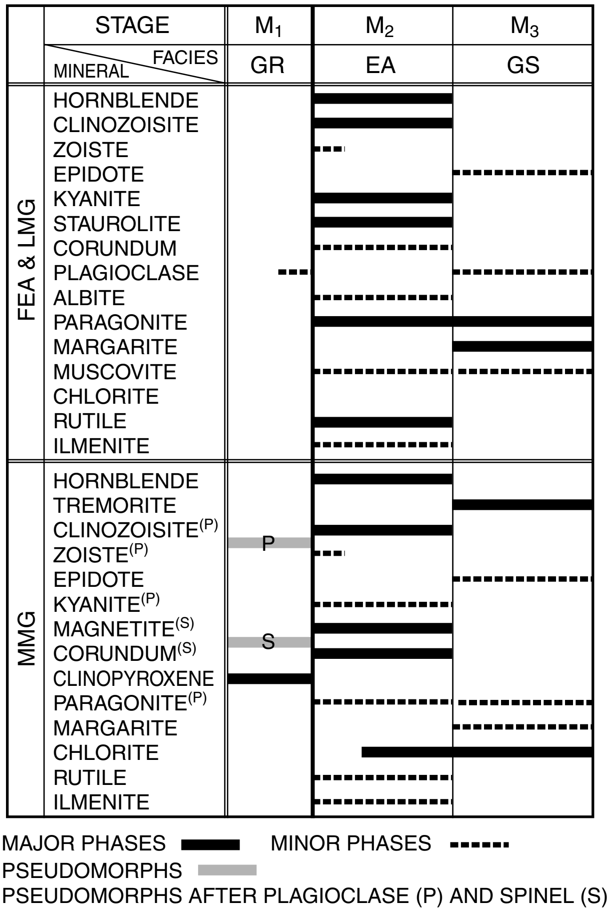

Fig. 2. Mineral parageneses for three stages of metamorphic recrystallization for foliated epidote–amphibolite and leucocratic metagabbro (FEA & LMG), and melanocratic metagabbro (MMG).

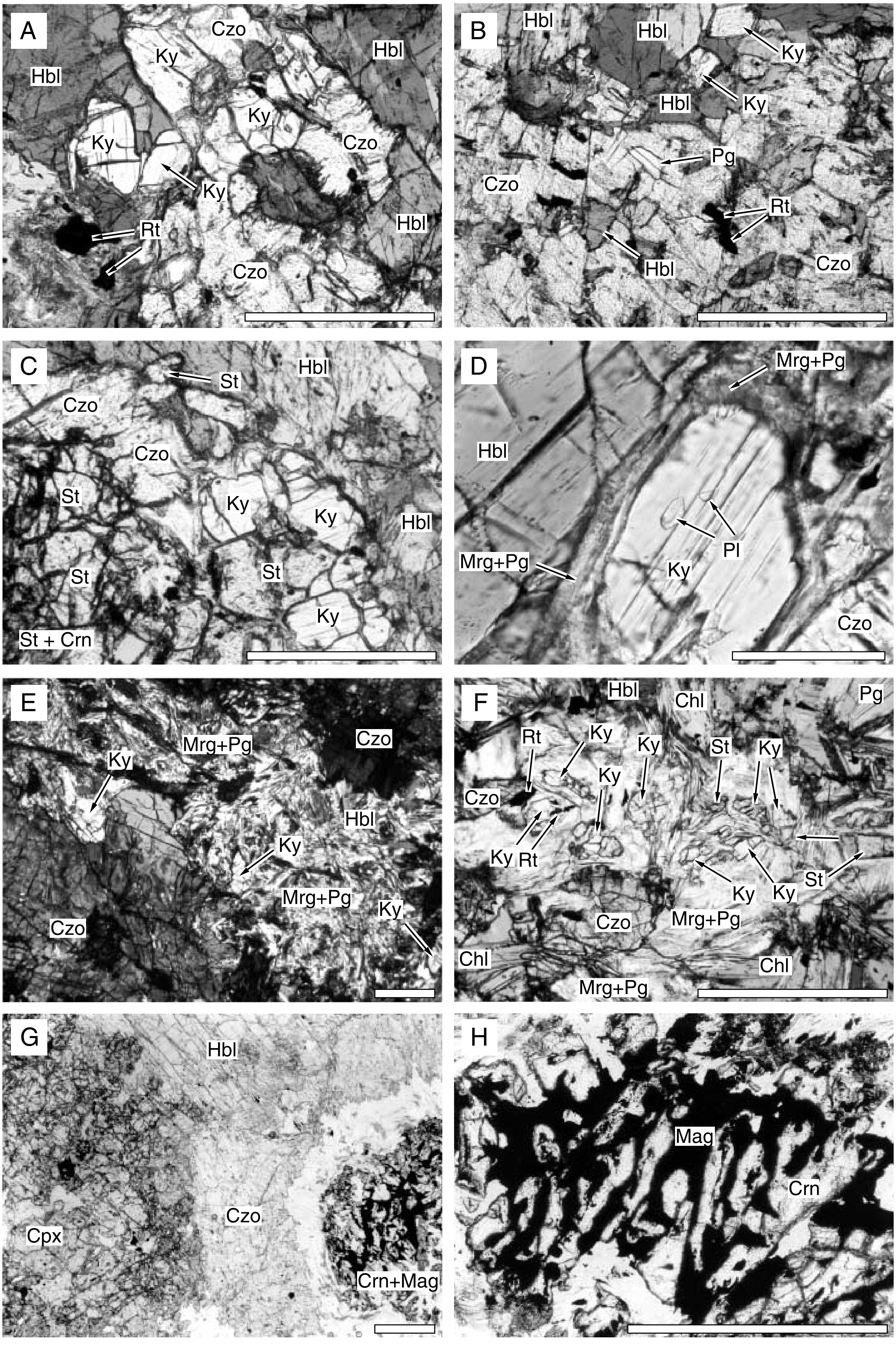
A
Czo
Ky
Hbl
Hbl
Ky
Ky
Czo
Ky
Rt
Hbl
Czo
B
Hbl
Hbl
Ky
Hbl
Ky
Pg
Czo
Rt
Hbl
Czo
C
St
Hbl
Czo
Czo
St
Ky
Ky
Hbl
St
St
Ky
St + Crn
D
Mrg+Pg
Hbl
Pl
Ky
Mrg+Pg
Czo
E
Czo
Mrg+Pg
Ky
Hbl
Ky
Mrg+Pg
Ky
Czo
F
Hbl
Chl
Pg
Rt
Ky
Ky
St
Ky
Czo
Ky
Ky
Rt
Ky
Ky
St
Czo
Mrg+Pg
Chl
Chl
Mrg+Pg
G
Hbl
Czo
Cpx
Crn+Mag
H
Mag
Crn

of ilmenite; some are rimmed by thin ilmenite. Retrograde M3 white mica occurs as coronitic aggregates around M2 kyanite (Fig. 3d). Chlorite and tiny plagioclase ($<$ 0.05 mm) occur rarely as M3 minerals with M3 margarite around M2 kyanite. M3 chlorite replaces M2 hornblende along the cleavage and staurolite in aggregates. The assemblage Mrg + Pg ± Ms + Chl ± Pl characterizes the M3 retrogression. In some samples, epidote overgrowths occur at interfaces between M2 clinozoisite and M3 hydrous minerals. Epidote may be a product of M3 or later.

LMG: leucocratic metagabbro

This rock type consists mainly of clinozoisite and kyanite with minor hornblende, margarite, paragonite, staurolite, rutile, chlorite, zoisite and muscovite. Rare ilmenite and apatite occur as accessories. Retrogression in this rock is more obvious than in the FEA. Coarse-grained clinozoisite (up to 15 mm) contains all M2 minerals as inclusions. Some kyanite grains show pale-blue pleochroism. Staurolite includes trace M2 paragonite. Kyanite is pseudomorphed by M3 margarite and paragonite (Fig. 3e,f). M3 muscovite occurs with M3 margarite and paragonite (Fig. 4). M3 margarite is associated with M3 chlorite and rare M3 plagioclase.

MMG: melanocratic metagabbro

This rock type consists mainly of hornblende, clinopyroxene, corundum-magnetite symplectite, clinozoisite and chlorite with minor kyanite, margarite, rutile and paragonite. Clinopyroxene is a relict mineral of M1; it occurs as equigranular grains (3–6 mm) partly replaced by M2 hornblende (Fig. 3g). The Crn–Mag symplectite has equidimensional shape (1–3 mm), and consists mainly of intergrowths of corundum and graphic magnetite with minor Zn-rich spinel (Fig. 3g,h); it was interpreted to be a pseudomorph after spinel of the M1 assemblage (Tsujimori & Ishiwatari, 2002). Moreover, mosaic aggregates of clinozoisite including kyanite and paragonite at interstices between M1 clinopyroxene and Crn–Mag symplectite were interpreted to be a pseudomorph after plagioclase of the M1 assemblage. Most kyanite inclusions in clinozoisite are replaced by M3 margarite. M3 chlorite replaces M2 hornblende, and occurs as chlorite-rich clots (3–5 mm), or aggregates surrounding the corundum-magnetite symplectite. Prismatic M3 epidote ($<$ 1 mm in length) and tiny magnetite are randomly oriented and frequently associated with the chlorite clots.

Fig. 3. Photomicrograph showing microtexture of the Ky–St bearing rocks. (a) The occurrence of M2 kyanite of the FEA. (b) M2 paragonite inclusions in clinozoisite of the FEA. (c) Staurolite aggregate associated with kyanite, clinozoisite and hornblende of the FEA; staurolite is associated with tiny corundum. (d) Plagioclase inclusions in M2 kyanite in equilibrium with Hbl and Czo of the FEA; M3 assemblage Mrg + Pg developed around Ky. (e) Coarse-grained pseudomorph consisting of M3 assemblage of Mrg + Pg after M2 kyanite of the LMG. (f) M3 assemblage Chl + Mrg + Pg developed around M2 Ky + St. (g) Relict M1 clinopyroxene and pseudomorph of Crn + Mag after spinel of the MMG; M2 hornblende replaces relict M1 Cpx and M2 clinozoisite occurs between Cpx and the Crn-Mag symplectite. (h) Enlarged view of corundum-magnetite symplectite after M1 spinel of the MMG.

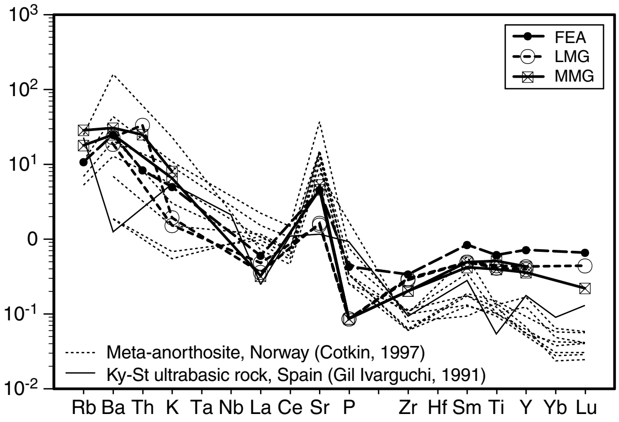

Fig. 4. N-MORB normalized incompatible element patterns of analyzed samples of FEA, LMG and MMG. For comparison, the element abundance patterns of meta-anorthosite of the Western Gneiss Region (Cotkin, 1997) and kyanite–staurolite-bearing rock from the Cabo Ortegal complex (NW Spain) (Gil Ibarguchi *et al*., 1991) are also illustrated.

Bulk-rock chemistry

One FEA, two LMG and two MMG samples were selected for geochemical study. Analysed bulk compositions are listed in Table 1. Major element analyses show that all lithologies contain extremely low SiO_2 (38.7–41.1 wt.%), high Al_2O_3 (18.9–25.5 wt.%), CaO (13.1–15.3 wt.%), and low $Na_2O + K_2O$ ($<$ 2.2 wt.%) with 48–66 mol.% normative anorthite and 16–28 mol.% olivine. The Mg/(Mg + Fe*) ratios range from 0.45 to 0.65 and increase in the order of FEA < LMG < MMG; Fe* = total Fe as Fe^{2+}. The FEA and LMG are enriched in Sr (402–479 p.p.m.) whereas the MMG shows enrichments of Ni (97–99 p.p.m.), Sc (135–143 p.p.m.), and Zn (166–224 p.p.m.). The N-MORB normalized trace element abundances of the analysed samples against the standard values of Sun & McDonough (1989) are shown in Fig. 4 for comparison. They are characterized by a high concentration of large ion lithophile (LIL) elements, and show similar patterns to those from meta-anorthosite of the Western Gneiss Region, Norway (Cotkin, 1997) and kyanite–staurolite-bearing rock from the Cabo Ortegal complex, NW Spain (Gil Ibarguchi *et al*., 1991). The low REE contents of the analysed samples suggest a cumulative origin. The bulk rock composition and the calculated norm suggest an origin from a troctolitic- and anorthositic cumulate with abundant anorthite-rich plagioclase.

MINERAL CHEMISTRY

Representative electron microprobe analysis of rock-forming minerals in the FPM are presented in Table 2.

Ca-amphibole

The structural formulae of amphibole are calculated based on O = 23 and the Fe^{2+}/Fe^{3+} ratio was estimated on the basis of total cation = 13, excluding Ca, Na and K (Leake *et al*., 1997). Most

Table 1. Bulk-rock compositions of the FPM.

Rock type	FEA	LMG		MMG	
Major-element compositions (in wt %)					
SiO_2	41.08	39.51	39.37	38.86	39.04
TiO_2	0.78	0.50	0.65	0.56	0.52
Al_2O_3	20.63	25.46	23.97	19.41	18.92
Fe_2O_3*	12.78	10.44	11.02	12.31	11.75
MnO	0.16	0.11	0.12	0.10	0.10
MgO	6.74	4.38	5.03	11.37	11.19
CaO	14.08	15.29	15.22	13.09	14.28
Na_2O	1.84	0.91	1.00	0.88	0.82
K_2O	0.36	0.58	0.47	0.14	0.11
P_2O_5	0.05	0.01	0.01	0.01	0.01
Total	98.45	97.18	96.85	96.72	96.73
Trace-element compositions (in ppm)					
Sc	43.3	30.1	34.5	143.1	135.5
V	536	415	425	633	610
Cr	33	59	76	64	52
Co	61	48	40	74	78
Ni	18	14	18	97	99
Cu	123	273	252	109	105
Zn	92	62	71	224	166
Rb	6	16	10	n.d.	n.d.
Sr	402	479	411	147	139
Y	20	10	12	12	11
Zr	25	15	15	21	22
Ba	156	192	157	144	117
La	2	n.d.	1	1	1
Sm	2	1	1	1	1
Eu	0.9	0.5	0.6	0.5	0.6
Lu	0.3	0.1	n.d.	0.2	n.d.
Th	1.0	3.0	n.d.	4.0	n.d.

*Total Fe as Fe_2O_3.
n.d. = not detected.

'hornblende' of the studied rocks are tschermakitic to pargasitic compositions containing up to 18 wt.% Al_2O_3, 3.4 wt.% Na_2O and 1.2 wt.% TiO_2, whereas actinolitic or tremolitic compositions are identified at the rim of relatively coarse-grained crystals in the MMG (Fig. 5). Individual hornblende grains in the FEA and LMG are unzoned, but their compositions are variable at the thin section scale. Minimum X_{Mg} [= $Mg/(Mg + Fe^{2+})$] values become higher in the order of FEA (0.59) < LMG (0.68) < MMG (0.73). Hornblende of the MMG contains significantly lower M4-site ($^{[M4]}Na$) than that in the FFM and LMG, apparently due to different bulk rock composition.

Epidote group minerals

The $X_{\mathrm{Fe}^{3+}}$ [= $Fe^{3+}/(Fe^{3+} + Al)$] of M2 clinozoisite in all lithologies varies from 0.10 to 0.24. The $X_{\mathrm{Fe}^{3+}}$ of a zoisite bleb is 0.03–0.07. M3 epidote of the FEA and MMG is characterized by distinctly high $X_{\mathrm{Fe}^{3+}}$ (0.26–0.29).

Kyanite

Pale-blue coloured kyanite in the LMG contains up to 1.3 wt.% Fe_2O_3, whereas other colourless kyanite has < 0.8 wt.% Fe_2O_3.

White mica

Chemical compositions of white mica are shown in Na (Pg)–K (Ms)–Ca (Mrg) diagrams of Fig. 6. M2 paragonite of the FEA contains slightly higher Mrg component (Mrg = 11–18 mol%) than that of the LMG and MMG (Mrg = 4–6 mol%); Ms component is < 10 mol%. M2 paragonite inclusions in staurolite of the LMG are characterized by extremely high Mrg component (Mrg = 36–47 mol%). M2 muscovite of the FEA is characterized by 6.2–6.3 Si p.f.u. (O = 22) and 17–24 mol% Pg. M3 paragonite of the FEA and LMG contains 2–14 mol% Mrg. M3 margarite shows a wide compositional range; Pg content varies from 7 to 34 mol%. M3 muscovite is characterized by 6.0–6.2 Si p.f.u. (O = 22) and < 10 mol% Pg.

Staurolite

The structural formulae of staurolite were calculated based on O = 46. Staurolite of the FEA contains a slightly higher X_{Mg} (0.19–0.36) but lower ZnO (0.7–1.6 wt.%) than that of LMG (X_{Mg} = 0.16–0.29, ZnO = 0.9–2.0 wt.%). The analysed staurolite shows good negative correlation of (Fe + Mg + Zn) against (Si + Ti + Al > 8) (Fig. 7). The correlation overlaps a substitution line of $(Mg + Fe)_{3+1.5x}Al_{18-x}Si_8O_{46}$ that represents magnesian staurolite (up to 0.61 X_{Mg}) in corundum-bearing amphibolite from an eclogitic metagabbro unit of the Sambagawa belt, SW Japan (Yokoyama & Goto, 1987).

Feldspar

M1 plagioclase inclusion in M2 kyanite of the FEA contains 26–34 mol% An. M2 albite in clinozoisite of the EFA contains < 5 mol% An (maximum 12 mol%). M3 plagioclase varies from 18 to 38 mol% An.

Clinopyroxene

M1 clinopyroxene of the MMG is Al-rich diopside that contains up to 8.5 wt.% Al_2O_3, up to 0.9 wt.% TiO_2 and < 0.34 wt.% Na_2O. The X_{Mg} varies from 0.78 to 0.94. The Al content decreases gradually toward the contact with clinozoisite.

Chlorite

M3 chlorite of the FEA and LMG is characterized by low Si (5.3–5.5 p.f.u. for O = 28) and high Al (5.1–5.8 p.f.u); X_{Mg} is 0.71–0.77 in the FEA, and 0.64–0.77 in the LMG. In the MMG, M3 chlorite around the corundum–magnetite symplectite is aluminous (Al p.f.u. = 5.6–5.9, O = 28) with X_{Mg} ranging from 0.70 to 0.75, whereas that in chlorite-rich clots shows a wide compositional range (Al p.f.u. = 5.0–5.9, X_{Mg} = 0.65–0.87).

Others

Rutile contains 0.3–0.8 wt.% Fe_2O_3. Corundum in staurolite aggregates of the FEA contains 0.8–1.2 wt.% Fe_2O_3. Corundum in the corundum-magnetite symplectite of the MMG contains 0.6–1.7 wt.% Fe_2O_3 and < 0.1 wt.% Cr_2O_3. Magnetite intergrown with the corundum contains 0.2–1.4 wt.% Al_2O_3 and 0.2–0.4 wt.% TiO_2. Zn-bearing spinel commonly shows exsolution texture; Ti-rich spinel lamellae (0.5–6.0 wt.% TiO_2, 7–14 wt.% ZnO and X_{Mg} = 0.24–0.51) are developed parallel to the {100} plane of Ti-poor spinel (< 0.2 wt.% TiO_2, 10–21 wt.% ZnO and X_{Mg} = 0.43–0.92). Ilmenite in the corundum-magnetite symplectite contains 2–7 wt.% MnO, whereas that in the FEA and LMG contains < 2 wt.% MnO.

METAMORPHIC CONDITIONS

Based on the observed petrographic features, a counter clockwise P–T evolution that passes from a medium-P granulite facies stage (M1) through a HP metamorphic

Table 2. Representative electron-microprobe analyses of rock-forming minerals in the FPM.

stage	M_1		M_2											M_3						
mineral	Cpx	Pl	Hbl			Ky	Czo	St	Crn	Pg	Ms	Crn	Ab	Tr	Mrg	Pg	Ms	Pl	Chl	Ep
rock type	MMG	FEA	FEA	LMG	MMG	FEA	FEA	FEA	FEA	FEA	FEA	FEA	FEA	MMG	LMG	LMG	LMG	FEA	LMG	MMG
SiO_2	47.72	60.99	42.21	44.96	42.95	37.20	38.31	27.67	0.00	46.07	46.66	0.00	68.06	52.49	30.38	46.22	44.87	58.38	26.45	38.25
TiO_2	0.70	0.11	0.38	0.94	1.11	0.00	0.08	0.17	0.01	0.12	0.95	0.01	0.04	0.33	0.00	0.09	0.08	0.09	0.03	0.21
Al_2O_3	8.31	24.32	17.05	13.03	15.88	62.84	27.60	53.62	98.79	40.09	33.34	98.79	19.74	5.52	50.63	39.71	37.57	25.87	23.13	22.73
Cr_2O_3	0.28	0.06	0.01	0.00	0.00	0.00	0.04	0.00	0.04	0.00	0.00	0.04	0.00	0.00	0.04	0.10	0.00	0.12	0.00	0.18
Fe_2O_3*	-	0.76	-	-	-	0.66	7.74	-	1.21	-	-	1.21	0.44	-	-	-	-	0.93	-	-
FeO**	5.88	-	13.82	13.39	8.39	-	-	11.66	-	0.65	1.93	-	-	6.88	0.70	0.90	0.64	-	17.73	13.45
MnO	0.11	0.00	0.15	0.14	0.07	0.01	0.25	0.43	0.03	0.05	0.20	0.03	0.09	0.08	0.00	0.00	0.00	0.12	0.059	0.04
MgO	12.70	0.00	9.77	12.15	14.60	0.00	0.13	2.83	0.02	0.15	1.23	0.02	0.00	18.77	0.49	0.00	0.32	0.00	19.62	0.00
CaO	24.55	5.94	10.38	10.90	12.33	0.01	22.87	0.04	0.06	1.58	0.11	0.06	0.61	12.31	11.65	0.81	0.07	7.83	0.11	23.60
Na_2O	0.00	8.23	2.92	2.59	2.30	0.00	0.02	-	0.01	6.52	1.79	0.01	11.44	0.74	1.10	7.22	0.63	7.07	0.01	0.00
K_2O	0.00	0.06	0.16	0.23	0.29	0.00	0.00	-	0.00	1.08	9.01	0.00	0.02	0.07	0.00	0.59	10.74	0.05	0.01	0.00
ZnO	-	-	-	-	-	-	-	0.89	-	-	-	-	-	-	-	-	-	-	-	-
Total	100.25	100.47	96.84	98.34	97.91	100.73	97.03	96.42	100.18	96.31	95.22	100.18	100.44	97.19	94.99	95.64	94.91	100.46	87.13	98.46
O=	6	8	23	23	23	5	25	46	3	22	22	3	8	23	22	22	22	8	28	25
Si	1.770	2.704	6.176	6.462	6.114	0.999	6.015	7.694	0.000	5.869	6.225	0.000	2.676	7.334	4.046	5.916	5.989	2.606	5.363	6.063
Ti	0.020	0.004	0.042	0.101	0.119	0.000	0.009	0.036	0.000	0.011	0.095	0.000	0.001	0.034	0.000	0.009	0.008	0.003	0.004	0.025
Al	0.363	1.271	2.940	2.207	2.663	1.988	5.108	17.573	1.982	6.019	5.242	1.982	1.310	0.909	7.947	5.990	5.911	1.361	5.527	4.247
Cr	0.008	0.002	0.001	0.000	0.000	0.000	0.004	0.000	0.000	0.000	0.000	0.000	0.001	0.000	0.004	0.010	0.000	0.004	0.000	0.022
Fe^{3+}	-	0.025	0.512	0.587	0.424	0.013	0.915		0.016	-	-	0.016	-	0.456	-	-	-	0.031	-	1.605
Fe^{2+}	0.182	-	1.180	1.022	0.575	-	-	2.712	-	0.069	0.215	-	0.017	0.349	0.078	0.096	0.072	-	3.008	-
Mn	0.003	0.000	0.019	0.017	0.008	0.000	0.034	0.101	0.000	0.005	0.023	0.000	0.000	0.010	0.000	0.000	0.000	0.005	0.010	0.006
Mg	0.702	0.000	2.132	2.603	3.097	0.000	0.030	1.173	0.000	0.028	0.245	0.000	0.011	3.909	0.098	0.000	0.063	0.000	5.931	0.000
Ca	0.976	0.282	1.627	1.679	1.880	0.000	3.846	0.012	0.001	0.216	0.016	0.001	0.290	1.843	1.663	0.111	0.010	0.375	0.023	4.008
Na	0.000	0.707	0.829	0.723	0.634	0.000	0.005	-	0.000	1.610	0.463	0.000	0.666	0.201	0.284	1.792	0.162	0.612	0.003	0.000
K	0.000	0.003	0.030	0.000	0.053	0.000	0.000	-	0.000	0.175	1.533	0.000	0.034	0.012	0.000	0.096	1.829	0.003	0.003	0.000
Zn	-	-	-	-	-	-	-	0.183	-	-	-	-	-	-	-	-	-	-	-	-
Total	4.025	4.999	15.485	15.401	15.567	3.001	15.965	29.301	2.001	14.003	14.057	2.001	5.008	15.056	14.120	14.020	14.043	5.000	19.872	15.975

*Total Fe as Fe_2O_3.
**Total Fe as FeO.

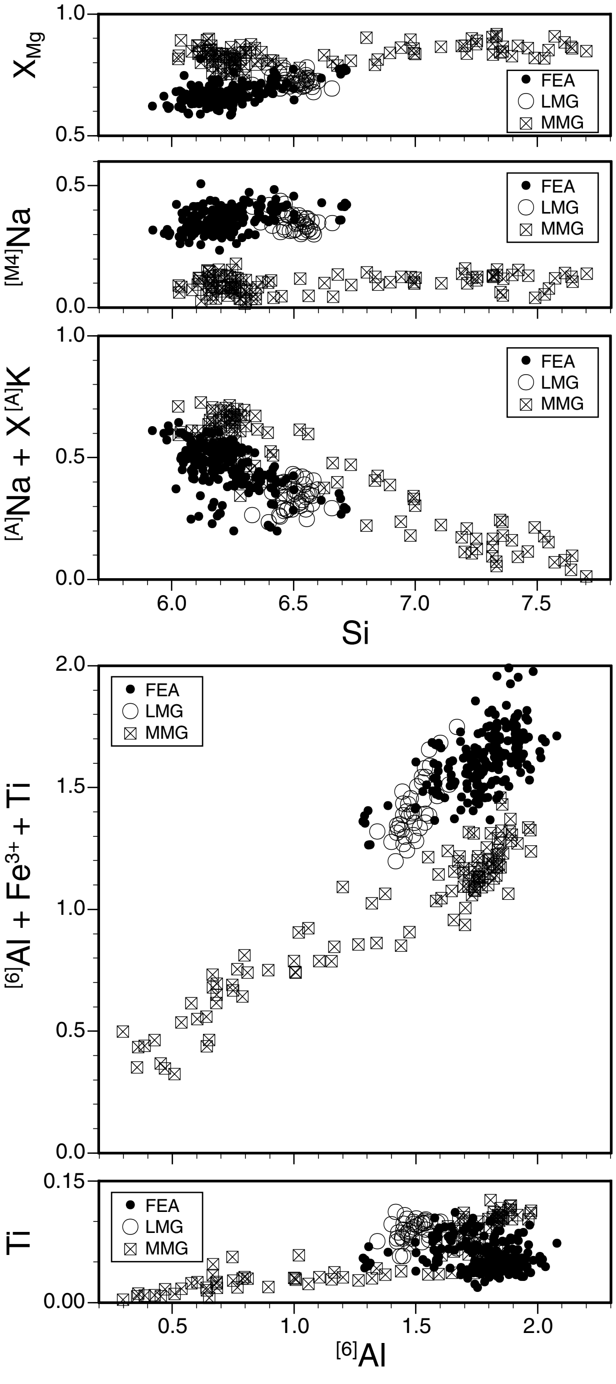

Fig. 5. Chemical compositions of Ca-amphibole on various plots (see text for details).

peak (M2) to retrogression (M3) was identified from the kyanite–staurolite-bearing rocks in the FPM (Fig. 2). No Fe–Mg exchange geothermobarometer is applicable for the observed mineral assemblage. Hence, metamorphic *P–T* conditions for each metamorphic stage are estimated based on available petrogenetic grids and phase equilibria. In this study,

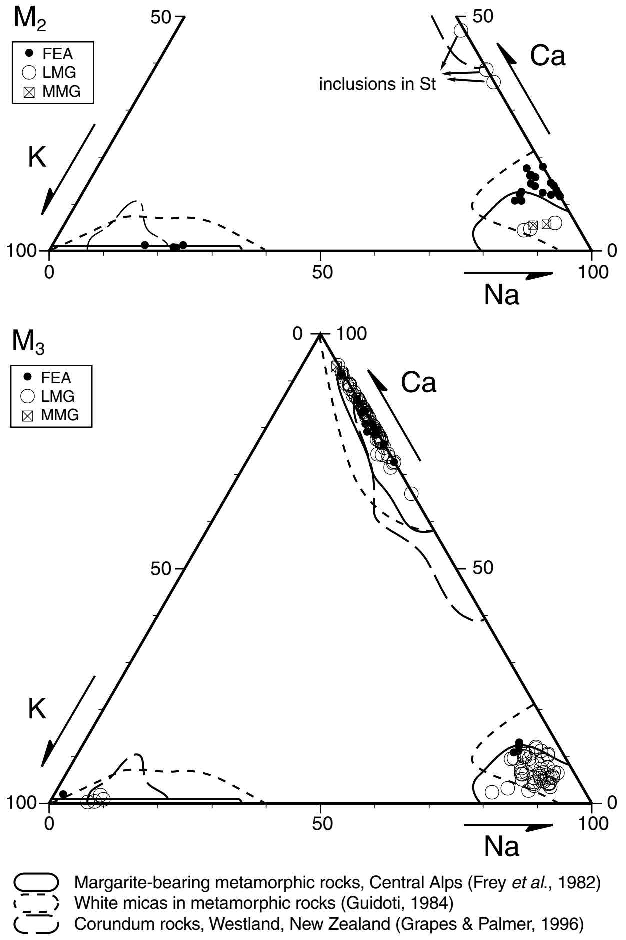

Fig. 6. K-Na-Ca plots of compositions of white micas from *M*2 and *M*3 stages. Compositional ranges of white micas by Frey *et al.* (1982), Guidotti, 1984) and Grapes & Palmer (1996) are also illustrated.

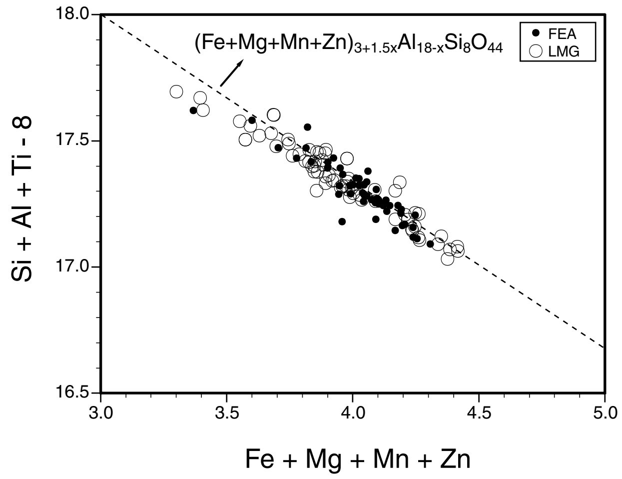

Fig. 7. Compositional variation of analyzed staurolite from FEA and LMG. The dashed line represents a substitution line $(Mg + Fe)_{3+1.5x}Al_{18-x}Si_8O_{46}$ of magnesian staurolite from the Sambagawa belt (Yokoyama & Goto, 1987).

calculations to obtain phase equilibria were carried out using version 1.1 of the software BAYES with an internally consistent thermodynamic dataset (Chatterjee *et al.*, 1998).

M1: relict granulite-facies stage

The M1 assemblage is preserved either as relict Al-rich diopside or as pseudomorphs after spinel and plagioclase. Al-rich diopside is an index mineral in lower crustal basic and ultrabasic granulites with the Cpx + Opx + Pl + Spl assemblage (e.g. Rivalenti *et al.*, 1981; Ishiwatari, 1985; Wilshire *et al.*, 1991; McGuire, 1994). Although no relict plagioclase occurs in the MMG, the presence of relict plagioclase within M2 kyanite of the FEA suggests its occurrence prior to kyanite crystallization. Orthopyroxene may also have originally been present in the M1, perhaps having been consumed in subsequent metamorphic overprints. The Al-rich Cpx + Spl (pseudomorph) + Pl (pseudomorph) assemblage suggests the medium-*P* granulite facies (0.8–1.3 GPa at > 800 °C), which is bracketed by the spinel-gabbro field in the system CaO-MgO-Al_2O_3-SiO_2 (Gasparik, 1984; Schmädicker, 2000). In the spinel–gabbro field, the Al content (Ca-tschermakite component) of clinopyroxene is higher than that in the olivine–gabbro and garnet–gabbro fields, and is strongly *T*-dependent (e.g. Obata, 1976; Gasparik, 1984). The Al content (up to 8.5 wt.% Al_2O_3) of relict clinopyroxene suggests a temperature of around 800–900 °C.

M2: kyanite–staurolite-bearing HP stage

The kyanite–staurolite-bearing M2 assemblage, Hbl + Czo + Ky ± St + Pg + Rt ± Ab ± Crn, characterizes the peak HP metamorphism of all FPM rock types. Since the FEA and MMG contain corundum instead of quartz, the equilibrium conditions were described by a model system projected from corundum. In the model CASH (CaO-Al_2O_3-SiO_2-H_2O) system with excess Crn + H_2O, the *P–T* limit of the Ky + Czo stability is defined by the following reactions (Fig. 8):

$$\mathrm{Dsp} = \mathrm{Crn} + \mathrm{H_2O}; \tag{1}$$

$$4\mathrm{An} + \mathrm{Crn} + \mathrm{H_2O} = 2\mathrm{Ky} + 2\mathrm{Czo}; \tag{2}$$

and

$$4\mathrm{Mrg} = 2\mathrm{Ky} + 2\mathrm{Czo} + 3\mathrm{Crn} + 3\mathrm{H_2O}. \tag{3}$$

The presence of paragonite, staurolite and albite provides more *P–T* constraints; the stability fields of these phases are bounded by the NASH (Na_2O-ASH) and FASH (FeO-ASH) reactions listed below:

$$\mathrm{Ab} + \mathrm{Crn} + \mathrm{H_2O} = \mathrm{Pg}; \tag{4}$$

$$\mathrm{Jd_{50}(Omp)} + \mathrm{Ky} + \mathrm{H_2O} = \mathrm{Pg}; \tag{5}$$

$$2\text{Fe-Cld} + 4\mathrm{Ky} + \mathrm{Crn} = \text{Fe-St} + 3\mathrm{H_2O}; \tag{6}$$

and

$$\mathrm{Jd} + \mathrm{Qtz} = \mathrm{Ab}. \tag{7}$$

The right hand sides of these reactions are stable in the M2. The stability fields shift towards the lower-*P* side and lower-*T* side with decreasing activities of clinozoisite and staurolite, respectively (Fig. 8). The *P–T* condition calculated using the software BAYES (Chatterjee *et al.*, 1998) with activities of minerals listed in Table 3 is 600–850 °C and 0.95–1.90 GPa.

On the other hand, inclusion of relict plagioclase in M2 kyanite has probably remained from the reaction (2) during cooling with hydration; this reaction constrains a *P–T* limit for the M2 to 550–800 °C and 1.1–1.9 GPa according to the BAYES calculation (Fig. 8). The compositional gap between M2 paragonite and M2 muscovite yields a temperature of *c.* 600 °C (Blencoe *et al.*, 1994). The Mrg-rich paragonite within staurolite may suggest a temperature of > 600 °C (Franz, 1977). The high Al (up to 18 wt.% Al_2O_3) and moderate Na (up to 3.4 wt.%) contents of hornblende further support the HP condition for these rocks (Ernst & Liu, 1998; Niida & Green, 1999).

M3: decompression stage

The M3 is documented by minor retrograde coronas armoured around M2 kyanite, and is characterized by the Mrg + Pg ± Pl + Chl assemblage. This assemblage is a breakdown product of Ky + Czo according to the following reactions (Fig. 8):

$$2\mathrm{Ky} + 2\mathrm{Czo} = \mathrm{Mrg} + 3\mathrm{An}; \tag{8}$$

and

$$2\mathrm{Ky} + 2\mathrm{Czo} + \mathrm{Ab} = \mathrm{Pg} + 4\mathrm{An}. \tag{9}$$

As both reactions (8) and (9) have gently positive *P–T* slopes, the M3 assemblage must involve a component of decompression; its *P–T* trajectory must cross these reaction curves. Staurolite was not replaced by the Cld + Ky assemblage during retrogression; hence reaction (6) also constrains the lower temperature limit to 450–500 °C at a maximum pressure of < 0.5 GPa for the M3 using the BAYES calculation (Fig. 8). The Pg–Mrg gap of the M3 mica suggests a temperature of *c.* 480 °C (Blencoe *et al.*, 1994).

DISCUSSION AND CONCLUSION

The FPM rocks preserve minor relict middle-*P* granulite facies (M1) assemblage of Cpx + Pl + Spl ± possible Opx. They have significantly recrystallized under the HP epidote–amphibolite facies metamorphism (M2) close to the eclogite facies and formed the Hbl + Czo + Ky ± St + Pg + Rt ± Ab ± Crn assemblage (M2). Subsequent decompression produced the Mrg + Pg ± Ms ± Pl + Chl

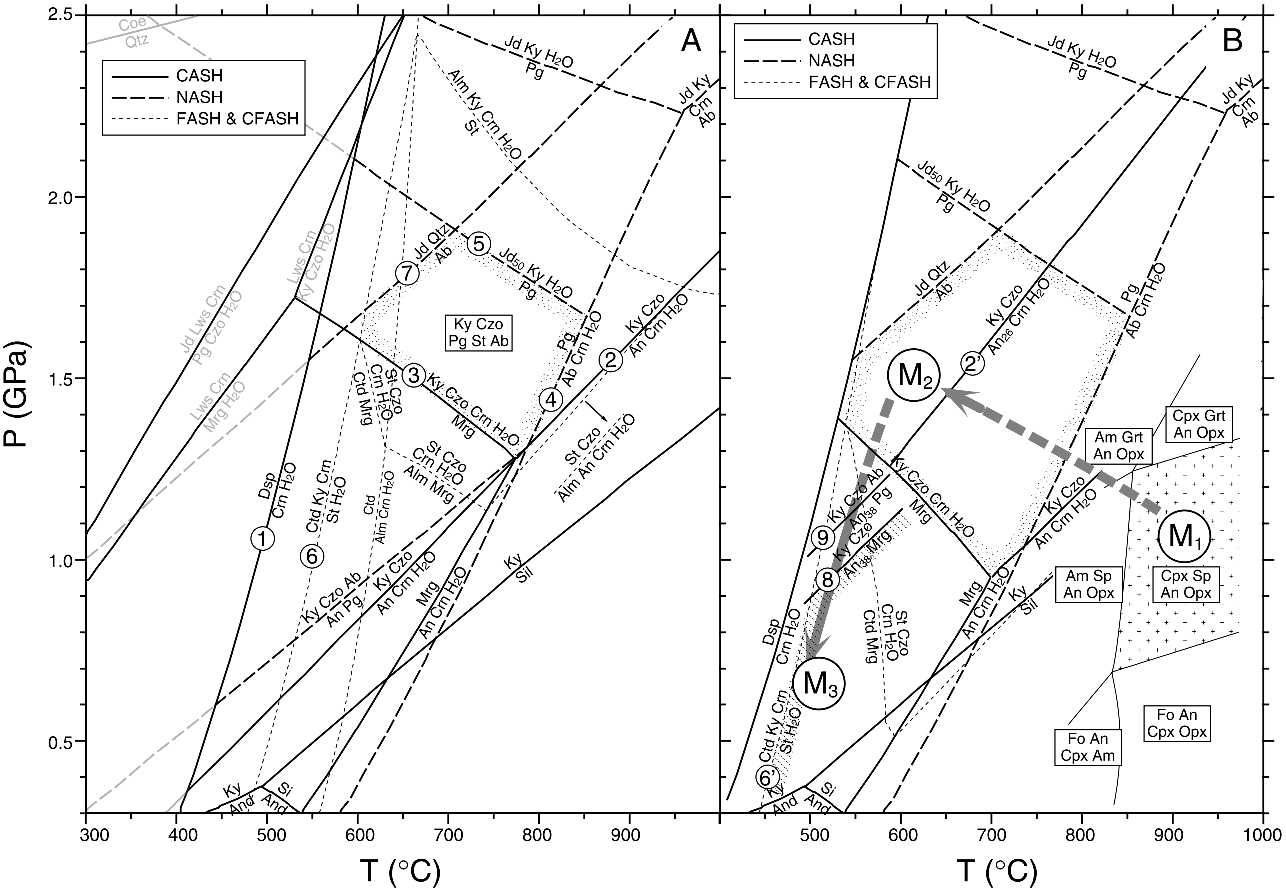

Fig. 8. *P–T* diagrams showing selected phase relationships and a qualitative *P–T* path of the FPM. All reactions are calculated by the software BAYES (Chatterjee *et al.*, 1998). (a) Stability field of the Ky + Czo + St + Ab assemblage with excess Crn and H_2O with end-member composition is shown in a shaded area. (b) A qualitative *P–T* path of the FPM. The selected reaction curves are calculated with the activities listed in Table 3. The reactions curves of (2') and (6') represent isopleths of the reactions (2) and (6) in (a), respectively. The petrogenetic grid defining the M1 condition is after Schmädicker (2000).

assemblage (M3). The *P–T* path for these three metamorphic events is shown in Fig. 8.

The estimated *P–T* conditions of the M_2 imply a geothermal gradient around 15 °C km^{-1}, indicating a subduction zone metamorphism. The decompression path from M2 to M3 is roughly isothermal and similar to some collision-type HP-UHP rocks (e.g. Maruyama *et al.*, 1996). The M3 may represent a greenschist facies overprint during exhumation; hornblende K/Ar ages of 443–403 Ma (Tsujimori *et al.*, 2000) may signify the timing of exhumation during the trajectory M2–M3. The timing of the M1 has not been dated, but it must be older than the K/Ar ages.

The presence of medium-*P* granulite-facies (M1) and the cooling trajectory to the HP metamorphism (M2) is an unusual feature, particularly in a Pacific-type orogen. Lower crustal granulites that were recrystallized and hydrated under HP or UHP metamorphism occur in many continental collision zones (e.g. Gil Ibarguchi *et al.*, 1991; Tenthorey *et al.*, 1996; Münttener *et al.*, 2000), because granulite facies rocks constitute major Precambrian continental crust. However, subducted 'allochthonous' granulites are less common in Pacific-type orogens. The relict granulite facies assemblage (Cpx + Opx + Pl + Spl ± Grt) in the eclogite unit of Cretaceous Sambagawa belt, Japan is a rare example. There, the relict granulites of basic to ultrabasic cumulate origin were recrystallized under the Cretaceous Sambagawa HP metamorphism to form unusual assemblages of Ky + Zo ± Grt and rare Ky + St + Crn (Yokoyama, 1980; Yokoyama & Goto, 1987). The metamorphic evolution of the FPM described above is similar to that of the Sambagawa 'granulites'.

Medium-*P* granulite facies conditions are attained at Moho depth beneath large oceanic plateaux (e.g. Saunders *et al.*, 1996). In fact, rare oceanic two-pyroxene granulites have been accreted as a minor component of ophiolite to the circum-Pacific orogen (e.g. Yakuno (SW Japan): Ishiwatari (1985); Tonshina (Alaska): DeBari & Coleman (1989); Bikin (Far East Russia): Vysotskiy, 1994); they have also been described as lower crustal xenoliths in the present-day oceanic plateau (Gregoire *et al.*, 1994). The bulk-rock chemistry implies

Table 3. End-member activities used in calculations of equilibria.

End-members	Formula	Activity Model	Activity
Czo	$Ca_3AlAl_2Si_3O_{12}(OH)$	X_{Al}^{M3} (Evans, 1990)	0.5
Ky	Al_2SiO_5	pure phase	1
An	$CaAl_2Si_2O_8$	1-binary ideal mixing (Holland and Powell, 1992)	0.61 (An_{38}); 0.39 (An_{26})
Mrg	$CaAl_4Si_2O_{10}(OH)_2$	pure phase	1
Lws	$CaAl_3Si_2O_7(OH)_2H_2O$	pure phase	1
Pg	$NaAl_3Si_3O_{10}(OH)_2$	pure phase	1
Ab	$NaAlSi_3O_{10}$	pure phase	1
Jd	$NaAlSi_2O_6$	X_{Jd}	1, 0.5 (Jd_{50})
Fe-St	$Fe_4Al_{18}Si_{7.5}O_{44}(OH)_4$	4-site Fe-Mg mixing (Worley and Powell, 1998)	0.2
Fe-Ctd	$FeAl_2SiO_5(OH)_2$	pure phase	1
Alm	$Fe_3Al_2Si_3O_{12}$	pure phase	1
Dsp	AlO(OH)	pure phase	1
Crn	Al_2O_3	pure phase	1
Qtz	SiO_2	pure phase	1
H_2O	H_2O	pure phase	1

that the protoliths of the Ky-St-bearing rocks in the FPM are correlative with troctolitic cumulus rocks, and coincident with cumulates of the 'non-island arc origin' ophiolites (Tsujimori & Ishiwatari, 2002). The relict granulite facies in both FPM and Sambagawa may provide constraints on the subduction of thick oceanic crust. Saunders *et al.* (1996) argued that the introduction of H_2O-rich fluid at the lower crustal part of an oceanic plateau allows transformation of gabbroic granulite to eclogite. They pointed out that the collision of thick oceanic crust causes a backward migration of the subduction zone, and consequently H_2O-rich fluid released from the subducting slab promotes transformation of suprasubduction zone ophiolitic rocks to eclogite. The unusual *P–T* evolution of the FPM may represent subduction of a thick-crustal oceanic plateau and subsequent exhumation.

Early Palaeozoic HP metamorphic rocks of the Kurosegawa belt (Maruyama & Ueda, 1974) and the Oeyama belt (Tsujimori *et al.*, 2000) provide a petrotectonic constraint for the earliest subduction event in the Japanese orogen. The HP rocks described in this paper occur in an early Palaeozoic subduction zone with geothermal gradient in the order of 15 °C km^{-1}. Such a relatively high geothermal gradient in the subduction zone has produced epidote–amphibolite facies metamorphic rocks. On the other hand, typical blueschists-eclogites with a low-geothermal gradient around 10 °C km^{-1} have been exhumed only after Devonian-Carboniferous time during a continuous subduction of colder oceanic lithosphere (Ueda *et al.*, 1980; Tsujimori & Itaya, 1999; Tsujimori, 2002). Such a difference and many other examples documented elsewhere led to a suggestion of secular cooling of Earth and subduction-zone geotherm by Maruyama *et al.* (1996).

ACKNOWLEDGEMENTS

This research was supported financially in part by a JSPS Research Fellowship for Young Scientists, and a Grant-in-Aid for JSPS Fellows to the first author. T. Itaya and A. Ishiwatari are thanked for helpful discussion. Preparation of this manuscript was supported by NSF EAR-0003355. We thank F. Spear and D. Pattison for their constructive comments.

REFERENCES

Arai, S., 1980. Dunite-harzburgite-chromitite complexes as refractory residue in the Sangun-Yamaguchi Zone, western Japan. *Journal of Petrology*, **21,** 141–165.

Arnold, J., Powell, R. & Sandiford, M., 2000. Amphibolites with staurolite and other aluminous minerals: calculated mineral equilibria in NCFMASH. *Journal of Metamorphic Geology*, **18,** 23–40.

Blencoe, J. G., Guidotti, C. V. & Sassi, F. P., 1994. The paragonite-muscovite solvus. II. Numerical geothermometers for natural, quasi binary paragonite-muscovite pairs. *Geochimica et Cosmochimica Acta*, **58,** 2277–2288.

Chatterjee, N. D., Krüger, R., Haller, G. & Olbricht, W., 1998. The Bayesian approach to an internally consistent thermodynamic database: theory, database, and generation of phase diagrams. *Contributions to Mineralogy and Petrology*, **133,** 149–168.

Cotkin, S. J., 1997. Igneous and metamorphic petrology of the eclogitic Seljeneset Meta-anorthosite and related jotunites, Western Gneiss Region, Norway. *Lithos*, **40,** 1–30.

Cotkin, S. J., Valley, J. W. & Essene, E. J., 1988. Petrology of a margarite-bearing meta-anorthite from Seljeneset, Nordfjord, western Norway: Implications for the P-T history of the Western Gneiss Region during Caledonian uplift. *Lithos*, **21,** 117–128.

DeBari, S. M. & Coleman, R. G., 1989. Examination of the deep levels of an island arc: evidence from the Tonsina ultramafic-mafic assemblage, Tonsina, Alaska. *Journal of Geophysical Research*, **94,** 4373–4391.

Ernst, W. G. & Liu, J., 1998. Experimental phase-equilibrium study of Al- and Ti-contents of calcic amphibole in MORB – semiquantitative thermobarometer. *American Mineralogist*, **83,** 952–969.

Evans, B. W., 1990. Phase relations of epidote-blueschists. *Lithos*, **25,** 3–23.

Franz, G., 1977. Determination of the miscibility gap on the solid solution series paragonite-margarite by means of the infrared spectroscopy. *Contributions to Mineralogy and Petrology*, **59,** 307–316.

Frey, M., Bucher, K., Frank, E. & Schwander, H., 1982. Margarite in the central Alps. *Schweizerische Mineralogische und Petrographische Mitteilungen*, **62,** 21–45.

Gasparik, T., 1984. Two-pyroxenes thermobarometry with new experimental data in the system CaO-MgO-Al_2O_3-SiO_2. *Contributions of Mineralogy and Petrology*, **87,** 87–97.

Gibson, G. M., 1979. Margarite in kyanite- and corundum-bearing anorthosite, amphibolites, and hornblendite from central Fiordland, New Zealand. *Contributions to Mineralogy and Petrology*, **68,** 171–179.

Gil Ibarguchi, J. I., Mendia, M. & Girardeau, J., 1991. Mg- and Cr-rich staurolite and Cr-rich kyanite in high-pressure ultrabasic rocks (Cabo Ortegal, northwestern Spain). *American Mineralogist*, **76,** 501–511.

Grapes, R. & Palmer, K., 1996. (Ruby-sapphire)-chromian mica-tourmaline rocks from Westland, New Zealand. *Journal of Petrology*, **37,** 293–315.

Gregoire, M., Mattielli, N., Nicollet, C., Cottin, J. Y., Leyrit, H., Weis, D., Shimizu, N. & Giret, A., 1994. Oceanic granulite from the Kerguelen Archipelago. *Nature*, **367,** 360–363.

Guidotti, C. V., 1984. *Micas in Metamorphic Rocks, Reviews in Mineralogy 13* (ed. Baily, S. W), 357–467. Mineralogical Society of America, Washington DC

Hayasaka, Y., Sugimoto, T. & Kano, T., 1995. Ophiolitic complex and metamorphic rocks in the Niimi-Katsuyama area, Okayama Prefecture. *Excursion Guidebook of 102nd Annual Meeting of the Geological Society of Japan*, 71–87 (in Japanese).

Holland, T. J. B. & Powell, R., 1992. Plagioclase feldspars: activity-composition relations based on Darkenís Quadratic Formalism and Landau theory. *American Mineralogist*, **77,** 53–61.

Ishiwatari, A., 1985. Granulite-facies metacumulates of the Yakuno ophiolite, Japan: Evidence for unusually thick oceanic crust. *Journal of Petrology*, **26,** 1–30.

Ishiwatari, A. & Tsujimori, T., 2003. Paleozoic ophiolites and blueschists in Japan and Russian Primorye in the tectonic framework of East Asia: a synthesis. *Island Arc*, **12,** 190–206.

Kretz, R., 1983. Symbols for rock forming minerals. *American Mineralogist*, **68,** 277–279.

Kuroda, Y., Kurokawa, K., Uruno, K., Kinugawa, T., Kano, H. & Yamada, T., 1976. Staurolite and kyanite from epidote-hornblende rocks in the Oeyama (Komori) ultramafic mass, Kyoto Prefecture, Japan. *Earth Sciences (Chikyu Kagaku)*, **30,** 331–333.

Kurokawa, K., 1975. Discovery of kyanite from epidote-amphibolite in the Oeyama ultramafic mass, inner zone of southwestern Japan. *Journal of Geological Society of Japan*, **81,** 273–274.

Kurokawa, K., 1985. Petrology of the Oeyama ophiolitic complex in the Inner Zone of Southwest Japan. *Science Report of Niigata University (Series E)*, **6,** 37–113.

Kuyumjian, R. M., 1998. Kyanite-staurolite ortho-amphibolite from the Chapada region, Goias, central Brazil. *Mineralogical Magazine*, **62,** 501–507.

Leake, B. E., Woolley, A. R., Arps, C. E. S., *et al.*, 1997. Nomenclature of amphiboles: Report of the subcommittee on amphiboles of the International Mineralogical Association, Commission on new minerals and mineral names. *American Mineralogist*, **82,** 1019–1037.

Maruyama, S., Liou, J. G. & Terabayashi, M., 1996. Blueschists and eclogites of the world, and their exhumation. *International Geology Review*, **38,** 485–594.

Maruyama, S. & Ueda, Y., 1974. Schist xenolith in ultrabasic body accompanied with Kurosegawa tectonic zone in eastern Shikoku and their K-Ar ages. *Journal of Japanese Association of Mineralogist, Petrologist and Economic Geologist*, **70,** 42–52. (in Japanese with English abstract).

Matsumoto, I., Arai, S. & Yamauchi, H., 1997. High-Al podiform chromitites in dunite-harzburgite complexes of the Sangun zone, central Chugoku district, Southwest Japan. *Journal of Asian Earth Sciences*, **15,** 295–302.

McGuire, A. V., 1994. Southern basin and range province crust–mantle boundary: evidence from gabbroic xenoliths, Wikieup, Arizona. *Journal of Geophysical Research*, **99,** 24263–24273.

Müntener, O., Hermann, J. & Trommsdorff, V., 2000. Cooling History and Exhumation of Lower-Crustal Granulite and Upper Mantle (Malenco, Eastern Central Alps). *Journal of Petrology*, **41,** 175–200.

Niida, K. & Green, D. H., 1999. Stability and chemical composition of pargasitic amphiboles in MORB pyrolite under upper mantle conditions. *Contributions to Mineralogy and Petrology*, **135,** 18–40.

Nishimura, Y., 1998. Geotectonic subdivision and areal extent of the Sangun belt, inner zone of Southwest Japan. *Journal of Metamorphic Geology*, **16,** 129–140.

Nishimura, Y. & Shibata, K., 1989. Modes of occurrence and K-Ar ages of metagabbroic rocks in the 'Sangun metamorphic belt', Southwest Japan. *Memoir of Geological Society of Japan*, **33,** 343–357. (in Japanese with English abstract).

Obata, M., 1976. The solubility of Al_2O_3 in orthopyroxenes in spinel and plagioclase peridotites and spinel pyroxenite. *American Mineralogist*, **61,** 804–816.

Rivalenti, G., Garuti, G., Rossi, A., Siena, F. & Sinigoi, S., 1981. Existence of different peridotite types and of a layered igneous complex in the Ivrea Zone of the Western Alps. *Journal of Petrology*, **22,** 127–153.

Saunders, A. D., Tarney, J., Kerr, A. C. & Kent, R. W., 1996. The formation and face of large oceanic igneous provinces. *Lithos*, **37,** 81–95.

Schmädicker, E., 2000. Phase relations in peridotitic and pyroxenetic rocks in the model systems CMASH and NCMASH. *Journal of Petrology*, **41,** 69–86.

Selverstone, J., Spear, F. S., Franz, G. & Morteani, G., 1984. High-pressure metamorphism in the SW Tauern Window, Austria: P-T paths from hornblende-kyanite-staurolite schists. *Journal of Petrology*, **25,** 501–531.

Spear, F. S. & Franz, G., 1986. PT evolution of metasediments from the Eclogite Zone, south-central Tauern Window, Austria. *Lithos*, **19,** 219–234.

Sun, S. S. & McDonough, W. E., 1989. Chemical and isotopic systematics of ocean basalts: implications for mantle composition and processes. In: (Saunders, A.D. & Norry, M.J., eds). *Magmatism in the Ocean Basins*, Geological Society of London, Special Publication, **42,** 313–345.

Tenthorey, E.A., Ryan, J. G. & Snow, E. A., 1996. Petrogenesis of sapphirine-bearing metatroctolites from the Buck Creek ultramafic body, southern Appalachians. *Journal of Metamorphic Geology*, **14,** 103–114.

Tsujimori, T., 1998. Geology of the Osayama serpentinite melange in the central Chugoku Mountains, southwestern Japan: 320 Ma blueschist-bearing serpentinite melange beneath the Oeyama ophiolite. *Journal of the Geological Society of Japan*, **104,** 213–231 (in Japanese with English abstract).

Tsujimori, T., 1999. Petrogenesis of the Fuko Pass high-pressure metacumulate from the Oeyama peridotite body, southwestern Japan: evidence for Early Paleozoic subduction metamorphism. *Memoir of Geological Society of Japan*, **52,** 287–302.

Tsujimori, T., 2002. Prograde and retrograde P-T paths of the Late Paleozoic glaucophane eclogite from the Renge metamorphic belt, Hida Mountains, southwestern Japan. *International Geology Review*, **44,** 797–818.

Tsujimori, T. & Ishiwatari, A., 2002. Granulite facies relics in the early Paleozoic kyanite-bearing ultrabasic metacumulate in the Oeyama belt, the Inner Zone of southwestern Japan. *Gondwana Research*, **5,** 823–835.

Tsujimori, T. & Itaya, T., 1999. Blueschist-facies metamorphism during Paleozoic orogeny in southwestern Japan: phengite K-Ar ages of blueschist-facies tectonic blocks in a serpentinite melange beneath Early Paleozoic Oeyama ophiolite. *Island Arc*, **8,** 190–205.

Tsujimori, T., Nishina, K., Ishiwatari, A. & Itaya, T., 2000. 403–443 Ma kyanite-bearing epidote amphibolite from the Fuko

Pass metacumulate in Oeyama, the Inner Zone of southwestern Japan. *Journal of Geological Society of Japan*, **106,** 646–649. (in Japanese with English Abstract).

Uda, S., 1984. The contact metamorphism of the Oeyama ultrabasic mass and the genesis of the 'cleavable olivine'. *Journal of Geological Society of Japan*, **90,** 393–410. (in Japanese with English Abstract).

Ueda, Y., Nakajima, T., Matsuoka, K. & Maruyama, S., 1980. K-Ar ages of muscovite from greenstone in the Ino Formation and schists blocks associated with the Kurosegawa tectonic zone near Kochi City, central Shikoku. *Journal of Japanese Association of Mineralogist, Petrologist and Economic Geologist*, **75,** 230–233. (in Japanese with English abstract).

Vysotskiy, S. V., 1994. High and low pressure cumulates of Paleozoic ophiolites in Primorye, eastern Russia. In: (Ishiwatari, A. *et al*., eds) *Circum-Pacific Ophiolites (Proceedings of the 29th IGC, Part D)*, pp. 145–162. VSP Publishers, Utrecht, the Netherlands.

Wilshire, H. G., McGuire, A. V., Noller, J. S. & Turrin, B. D., 1991. Petrology of lower crustal and upper mantle xenoliths from the Chima Volcanic Field, California. *Journal of Petrology*, **32,** 169–200.

Worley, B. A. & Powell, R., 1998. Singularities in the system NCKFMASH (Na_2O-CaO-K_2O-FeO-MgO-Al_2O_3-SiO_2-H_2O). *Journal of Metamorphic Geology*, **16(2),** 169–188.

Yokoyama, K., 1980. Nikubuchi peridotite body in the Sanbagawa metamorphic belt; thermal history of the Al-pyroxene-rich suiteí peridotite body in high pressure metamorphic terrain. *Contributions to Mineralogy and Petrology*, **73,** 1–13.

Yokoyama, K. & Goto, A., 1987. Mg-rich staurolite from the Iratsu epidote amphibolite body, central Shikoku. *Journal of Japanese Association of Mineralogist, Petrologist and Economic Geologist*, **82,** 281–290.

Received 28 March 2003; revision accepted 12 January 2004.